Method for Measuring Thickness of Dielectric Films Using Microdielectric Fringe-Effect Sensors

ARTICLE *in* ANALYTICAL CHEMISTRY · JUNE 2006

Impact Factor: 5.64 · DOI: 10.1021/ac050770z · Source: PubMed

3 AUTHORS, INCLUDING:

Mikhail Skliar

University of Utah

89 PUBLICATIONS **798** CITATIONS

SEE PROFILE

Anal. Chem. **2006,** *78,* 3242−3248

Method for Measuring Thickness of Dielectric Films Using Microdielectric Fringe-Effect Sensors

Yunn-Hong Choi, Prashant Tathireddy, and Mikhail Skliar*

Department of Chemical Engineering, University of Utah, Salt Lake City, Utah 84112

A method for noninvasive thickness measurements of dielectric films using fringe-effect (FE) sensors is developed and experimentally validated. The fringing electrical field, created by electrodes microfabricated at the film substrate, depends on the film thickness and dielectric permittivity of the film under test (FUT). The unknown film thickness is estimated by matching the theoretical prediction of thickness-dependent sensor admittance with the measured value. In the case of FE sensors with spatially periodic, interdigitated electrode (IDE) configuration, the admittance prediction is simplified, which allows for the real-time measurements of changing thickness. The developed method can be used to continuously measure the changing dielectric permittivity of the FUT material, which makes it possible to determine the thickness of films of changing dielectric properties, caused by chemical or other transformations. The application of the developed method is demonstrated experimentally by measuring the thickness of silicon nitride film deposited in several increments on the quartz substrate of the IDE sensor. In the expected range of sensor sensitivity, the results show an excellent agreement with the independent thickness measurements.

Accurate measurement of film thickness is an important problem in a wide range of applications.[1−6] For example, such measurements are fundamental in microfabrication processes, such as chemical vapor deposition, molecular beam epitaxy, thermal oxidation, diffusion, and sputtering,[2] and are essential in many biological and biomedical applications.[3]

Various physical principles can be used to noninvasively estimate film thickness, including interferometry,[1,2] sample weighing,[7] X-ray photoelectron spectroscopy,[8] wavelength scanning,[9] ellipsometry,[10,11] coherence tomography,[12] and analytical electron microscopy.[13] Most of the available techniques are limited to certain types of films or may not be suitable for making in situ measurements in real time.

In this paper, we develop a novel thickness measurement method based on the admittance measurements of microdielectric fringe-effect (FE) sensors. The FE sensor consists of an array of planar microelectrodes, fabricated on an insulating substrate. The material under test (MUT) in contact with the sensor is probed by applying an ac potential of amplitude $|\varphi_d|$ to the driven electrodes. The resulting total current, I, through sensing electrodes is measured and used to calculate sensor admittance. Figure 1 illustrates this arrangement and shows a cross-sectional view of an interdigitated electrode (IDE) sensor and a sample, consisting of a thin film under test (FUT) and semi-infinite layer (SIL), which have dielectric permittivities ϵ^*_{fut} and ϵ^*_{sil}, respectively. When dielectric properties of FUT and SIL materials are dissimilar, the "fringing" distribution of the probing electric field through the sample, created by a sensor, depends on the film thickness, T_1. Consequently, the sensor admittance (eq 4) is also a function of T_1.

The central idea of the proposed method is to estimate T_1 by matching thickness-dependent theoretical prediction of the sensor admittance, $\mathbf{Y}_{sen}$, with the measured admittance, $\mathbf{Y}_m$. The formal statement of the problem is to find T_1, which solves the following optimization problem:

$$\min_{T_1} ||\mathbf{Y}_m - \mathbf{Y}_{sen}(T_1)|| \tag{1}$$

The solution can be found by, first, predicting $\mathbf{Y}_{sen}$ as a function of T_1 (a direct problem) and then finding the thickness T_1, which minimizes the difference between the predicted and the measured sensor admittances (an inverse problem). Both, direct and inverse problems are computationally intensive in the general case of FE sensors of an arbitrary geometry and electrode configuration. However, as demonstrated in the Direct Problem section, the computational complexity is significantly reduced for IDE sensors because of the spatial periodicity of the excitation field.

The measured sensor admittance includes contributions from stray elements introduced by contact impedance, interconnecting

* To whom correspondence should be addressed. E-mail: mikhail.skliar@utah.edu.

(1) Yang, K. H. *J. Appl. Phys.* **1988**, *64*, 4780.
(2) Boebel, F. G.; Gesellschaft, F.; Bonnes, U.; Frohmader, K. P. *IEEE/CHMT European International Electronic Manufacturing Technology Symposium*; 1991; pp 197−201.
(3) Martin, C.; Meister, J. J.; Marcel, A.; Farine, P. A. *IEEE Trans. Signal Process.* **1992**, *40*, 1819.
(4) Tosaka, H.; Minami, K.; Esashi, M. *J. Micromech. Microeng.* **1995**, *5*, 41.
(5) Lobo, R. F. M.; da Silva, M. A. P.; Raposo, M.; Faria, R. M.; Oliveira, O. N. *Nanotechnology* **1999**, *10*, 389.
(6) Pekker, D.; Pekker, L. *Thin Solid Film* **2003**, *425*, 203.
(7) Modreanu, M.; Cosmin, P.; Cosmin, S.; Cobianu, C.; Dunare, C. *Proceedings of the International Semiconductor Conference, CAS*; 1996; Vol. 2, p 409.
(8) Ando, K.; Ishitani, A.; Hamano, K. *Appl. Phys. Lett.* **1991**, *59*, 1081.
(9) Koysal, O.; Onal, D.; Ozder, S.; Ecevit, F. N. *Opt. Commun.* **2002**, *205*, 1.
(10) Kasko, I.; Kal, S.; Ryssel, H. *Microelectron. Eng.* **1997**, *37−38*, 455.
(11) Kal, S.; Kasko, I.; Ryssel, H. *IEEE Electron. Device Lett.* **1998**, *19*, 127.
(12) Hitzenberger, C. K.; Baumgartner, A.; Fercher, A. F. *Opt. Commun.* **1998**, *154*, 179.
(13) Williams, D. B.; Watanabe, M.; Papworth, A. J.; Li, J. C. *Thin Solid Film* **2003**, *424*, 50.

10.1021/ac050770z CCC: $33.50
Published on Web 04/07/2006

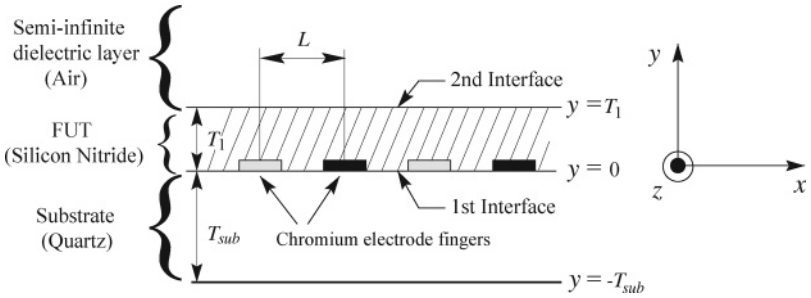

Figure 1. Cross-sectional view of an IDE sensor with the sample consisting of a FUT and a SIL in which the FUT evolves.

leads, variation in electrode geometry, and other factors. The theoretical prediction of stray contributions, $\mathbf{Z}_{stray}$, is difficult, if not impossible. Therefore, a practically useful implementation of the central idea of finding T_1 must be modified to account for $\mathbf{Z}_{stray}$.

The procedure for estimating unknown stay contribution using the admittance measurements of the FE sensor with a known sample is given in the Stray Contributions section. With known $\mathbf{Z}_{stray}$, the optimization problem (1) is modified and T_1 is found by minimizing the difference between $\mathbf{Y}_m$ and the stray-adjusted prediction, $\mathbf{Y}'_{sen}(T_1)$, given by the following equation:

$$\mathbf{Y}'_{sen}(T_1) = \left[\frac{1}{\mathbf{Y}_{sen}(T_1)} + \mathbf{Z}_{stray}\right]^{-1} \tag{2}$$

An equivalent way to account for the effect of $\mathbf{Z}_{stray}$ is to minimize the difference between stray-adjusted measurements, $\mathbf{Y}'_m$, and theoretical predictions $\mathbf{Y}_{sen}$.

For low-loss dielectrics, the measured admittance is often expressed as

$$\mathbf{Y}_m(\omega) = \frac{1}{R_m(\omega)} + j\omega C_m(\omega) \tag{3}$$

where ω is the angular excitation frequency and C_m and R_m are the measured capacitance and resistance of the FE sensor, respectively. Both R_m and C_m depend on film thickness. Because it is difficult to accurately measure very high resistances, a particular implementation of the method, outlined in Estimation of the Film Thickness section, is to estimate T_1 by minimizing the error between the measured capacitance C_m and its stay-adjusted theoretical prediction $C'_{sen}(T_1)$. For materials with higher conductive losses, the thickness can be estimated by obtaining the best possible match between $R'_{sen}(T_1)$ and the measured R_m.

After presenting the results of the experimental validation of the proposed method, the paper is concluded with the discussion of the advantages and limitations of the developed approach.

METHOD

1. Direct Problem. Consider a dielectric film of thickness T_1 and permittivity ϵ^*_{fut}, deposited on the sensor substrate of thickness T_{sub} and permittivity ϵ^*_{sub}. Assume that the bottom of the sensor substrate is grounded, $\varphi(x, y = -T_{sub}, z) = 0$, and that the dielectric permittivity of the semi-infinite layer, ϵ^*_{sil}, is known. Figure 1 illustrates the described configuration for the specific case of a semi-infinite layer of dry air and silicon nitride FUT deposited on the quartz substrate of the IDE sensor.

For an arbitrary FE sensor, the theoretical prediction of sensor admittance is given by the following integral, calculated over the surface S of sensing electrodes:

$$\mathbf{Y}_{sen} = \frac{I}{\hat{\varphi}_d} = \frac{j\omega\epsilon_0}{|\varphi_d|}\oint_S \epsilon^* \mathbf{E}\, d\bar{\mathbf{s}} \tag{4}$$

where $\hat{\varphi}_d = |\varphi_d| \exp(j\omega t)$ is the sinusoidal potential of frequency ω, applied to the driven electrodes with sensing electrodes kept grounded; $I = I_{sub} + I_{sam}$ is the total electric current through the sensor substrate and the sample (in Figure 1, FUT plus the semi-infinite layer); the complex dielectric permittivity ϵ^* is equal to either ϵ^*_{sub}, ϵ^*_{fut}, or ϵ^*_{sil} depending on the coordinate y; ϵ_0 is the dielectric constant of free space; and $\mathbf{E}$ is the complex vector of electric field created by the FE sensor. The electric field can be calculated if the potential distribution, φ, is known inside the substrate, FUT, and the semi-infinite layer. In electroquasistatic approximation of Maxwell equations, potential distribution satisfies the Laplace equation, $\nabla^2\varphi = 0$, and is continuous across all interfaces.[14]

Assume that the potential distribution is two-dimensional, $\varphi(x, y, z) = \varphi(x, y)$, which implies a two-dimensional electrical field, $\mathbf{E} = (E_x, E_y)$. For IDE sensors of a high ratio of the electrode length in z direction, L_{sen}, to their width in x direction, such an assumption leads to a minimal error. Furthermore, we will ignore the thickness of electrodes, which is typically much smaller than other dimensions of the sensor. Under these assumptions, for periodically structured FE sensors, we can derive an explicit expression for $\mathbf{Y}_{sen}$. We begin by expressing the potential distribution as an infinite series:

$$\varphi(x, y) = \sum_{n=0}^{\infty} \varphi_n(x, y) \tag{5}$$

where each component φ_n must satisfy the Laplace equation: $\nabla^2\varphi_n = 0$, $n = 0, 1, 2, \ldots$.

The solution for φ_n in the limiting case of a single interface at $y = 0$ (obtained when $T_1 = 0$ or $T_1 = \infty$) was previously obtained in ref 15, where the potential distribution was then used to develop a standard-independent method for quantitative dielectroscopic measurements of the permittivity of the semi-infinite layer of the

(14) Cheng, D. K. *Field and Wave Electromagnetics*; Addison-Wesley Publishing Co., Inc.: New York, 1983.
(15) Choi, Y.-H.; Skliar, M. *Anal. Chem.* **2005**, *77*, 871.

MUT. Using a similar approach for the system with two interfaces at $y = 0$ and $y = T_1$, depicted in Figure 1, but omitting mathematical details, the following solution is found:

$$\varphi_n(x, y) = \begin{cases} [\coth(k_n T_{sub})\ \sinh(k_n y) + \cosh(k_n y)]\varphi_n^{(1)}(x), & -T_{sub} \le y \le 0 \\ \dfrac{\sinh(k_n y)}{\sinh(k_n T_1)}\varphi_n^{(2)}(x) - \dfrac{\sinh[k_n(y - T_1)]}{\sinh(k_n T_1)}\varphi_n^{(1)}(x), & 0 \le y \le T_1 \\ -\{\sinh[k_n(y - T_1)] - \cosh[k_n(y - T_1)]\}\varphi_n^{(2)}(x), & T_1 \le y \le \infty \end{cases} \quad (6)$$

where $k_n = n\pi/L$, L is the distance between the centers of the two adjacent electrodes and the infinite summations of $\varphi_n^{(1)}$ and $\varphi_n^{(2)}$ are equal to the potentials at the two interfaces:

$$\varphi(x, y = 0) = \sum_{n=0}^{\infty}\varphi_n^{(1)}(x) \text{ and } \varphi(x, y = T_1) = \sum_{n=0}^{\infty}\varphi_n^{(2)}(x)$$

We now consider a series solution for the normal component of the electric field:

$$E_y = \sum_{n=0}^{\infty}E_{y,n}$$

Since $\mathbf{E} = -\nabla\varphi$, we obtain from eq 6 that

$$E_{y,n}(x, y) = \begin{cases} -k_n[\coth(k_n T_{sub})\ \cosh(k_n y) + \sinh(k_n y)]\varphi_n^{(1)}(x), & -T_{sub} \le y \le 0 \\ -k_n\dfrac{\cosh(k_n y)}{\sinh(k_n T_1)}\varphi_n^{(2)}(x) + k_n\dfrac{\cosh[k_n(y - T_1)]}{\sinh(k_n T_1)}\varphi_n^{(1)}(x), & 0 \le y \le T_1 \\ k_n\{\cosh[k_n(y - T_1)] - \sinh[k_n(y - T_1)]\}\varphi_n^{(2)}(x), & T_1 \le y \le \infty \end{cases} \quad (7)$$

Therefore, at the first interface $y = 0$:

$$E_{y,n}^{(1)a}(x) = E_{y,n}(x, 0^+) = -\frac{k_n}{\sinh(k_n T_1)}\varphi_n^{(2)} + k_n \coth(k_n T_1)\varphi_n^{(1)} \quad (8)$$

$$E_{y,n}^{(1)b}(x) = E_{y,n}(x, 0^-) = -k_n \coth(k_n T_{sub})\varphi_n^{(1)} \quad (9)$$

where superscript a and b denote the location immediately above ($y = 0^+$) and below ($y = 0^-$) the interface, respectively. Similarly, at the second interface $y = T_1$:

$$E_{y,n}^{(2)a}(x) = E_{y,n}(x, T_1^+) = k_n\varphi_n^{(2)} \quad (10)$$

$$E_{y,n}^{(2)b}(x) = E_{y,n}(x, T_1^-) = -k_n \coth(k_n T_1)\varphi_n^{(2)} + \frac{k_n}{\sinh(k_n T_1)}\varphi_n^{(1)} \quad (11)$$

Each component of the series solution at both interfaces must also satisfy the following continuity conditions:[14]

$$\epsilon_{fut}^* E_{y,n}^{(1)a} = \epsilon_{sub}^* E_{y,n}^{(1)b} \quad (12)$$

$$\epsilon_{sil}^* E_{y,n}^{(2)a} = \epsilon_{fut}^* E_{y,n}^{(2)b} \quad (13)$$

which allows us to establish the relationship between the components of the series representations of potentials $\varphi_n^{(1)}$ and $\varphi_n^{(2)}$ at the two interfaces:

$$\varphi_n^{(2)} = \frac{\epsilon_{fut}^*}{\sinh(k_n T_1)[\epsilon_{sil}^* + \epsilon_{fut}^* \coth(k_n T_1)]}\varphi_n^{(1)} \quad (14)$$

Using 14 in eq 8, one obtains that

$$E_{y,n}^{(1)a}(x) = s_n(k_n\varphi_n^{(1)}(x)) \quad (15)$$

where, for a finite, nonzero T_1,

$$s_n = \coth(k_n T_1) - \frac{1}{\sinh^2(k_n T_1)}\left[\frac{\epsilon_{fut}^*}{\epsilon_{sil}^* + \epsilon_{fut}^* \coth(k_n T_1)}\right] \quad (16)$$

For large T_1, $s_n \to 1$. On the other hand, as $T_1 \to 0$, ϵ_{fut}^* becomes equal to the permittivity of a semi-infinite layer, and s_n again tends to 1. Therefore, as expected, when $T_1 = \infty$ or 0, the solution with two interfaces is reduced to the case of a single sensor−sample interface, previously considered in ref 15.

The periodicity and even symmetry of the IDE sensor geometry implies that the potential at the first interface can be expressed as the following Fourier cosine series:

$$\varphi(x, y = 0) = \sum_{n=0}^{\infty}\varphi_n^{(1)} = \sum_{n=0}^{\infty}f_n \cos(k_n x) \quad (17)$$

where f_n are the Fourier coefficients. The truncated expression for the normal components of the electric field at the first interface, needed to obtain theoretical prediction of the sensor admittance, is given by the following Fourier series solution:

$$E_y^{(1)a} = \sum_{n=0}^{m}E_{y,n}^{(1)a} = \sum_{n=0}^{m}s_n[k_n f_n \cos(k_n x)] \quad (18)$$

$$E_y^{(1)b} = \sum_{n=0}^{m}E_{y,n}^{(1)b} = -\sum_{n=0}^{m}k_n \coth(k_n T_{sub})f_n \cos(k_n x) \quad (19)$$

which depend on yet undetermined Fourier coefficients, f_n.

1.1. Potential Profile at the FUT−Substrate Interface. The expression for the electrical potential at a single interface between the sensor substrate and semi-infinite sample ($T_1 = \infty$ or 0) was obtained in ref 15. Following the same approach, it can be shown that, in the case of two interfaces at $y = 0$ and $y = T_1$, the potential at the film−substrate interface satisfies the following expression:

$$[\epsilon_{sub}^*\mathbf{B} + \epsilon_{fut}^*\mathbf{A}]\mathbf{F} = |\varphi_d|[\epsilon_{sub}^*\mathbf{BM} + \epsilon_{fut}^*\mathbf{AM}]\Phi = 0_1 \quad (20)$$

where $\mathbf{F} = [f_0, f_1, ..., f_m]^T$ is the vector of complex Fourier

coefficients; $\Phi = [1, \varphi_0(x_1), \varphi_0(x_2), ..., \varphi_0(x_i), ..., \varphi_0(x_k)]^T$ is the vector of scaled complex values of the potential distribution ($\varphi_0(x_i) = \varphi(x_i, 0)/|\varphi_d|$), evaluated in k uniformly spaced points at the substrate−FUT interface with coordinates $x_i = (L/[2(k + 1)])i + L/4$, $i = 1, ..., k$; the real matrices $\mathbf{M} \in \mathcal{R}^{(m+1)\times(k+1)}$ and $\mathbf{B} \in \mathcal{R}^{k\times(m+1)}$ are given in ref 15 by eqs 10 and 15, respectively; 0_1 is the k-dimensional zero vector; the complex matrix $\mathbf{A} \in \mathcal{C}^{k\times(m+1)}$ is defined by its components:

$$A_{i,n+1} = s_n\left[\sin\left(k_n\frac{x_{i+1} + x_i}{2}\right) - \sin\left(k_n\frac{x_i + x_{i-1}}{2}\right)\right] \quad (21)$$

which depend on FUT thickness T_1.

To solve for unknown components of Φ and Fourier coefficients, $\mathbf{F}$, define the matrix $\mathbf{T} = [\epsilon^*_{sub}\mathbf{BM} + \epsilon^*_{fut}\mathbf{AM}]$ and partition it as $\mathbf{T} = [\mathbf{T}_1\ \mathbf{T}_2]$, where the column vector $\mathbf{T}_1 = \mathbf{T}(:, 1)$ and the matrix $\mathbf{T}_2 = \mathbf{T}(:,2{:}k + 1)$. In this new notation, eq 20 can be written as

$$\mathbf{T}_2\Phi_p = -\mathbf{T}_1 \quad (22)$$

where we took into account that $\Phi(1) = 1$ and gathered unknown values of the scaled potential in collocation points x_i at $y = 0$ into the vector $\Phi_p = \Phi(2{:}k + 1)$. If T_1, T_{sub}, and the dielectric permittivities ϵ^*_{fut}, ϵ^*_{sil}, ϵ^*_{sub} are known, then $\mathbf{T}_1$ and $\mathbf{T}_2$ can be calculated, and eq 22 can be solved for unknown interfacial potentials Φ_p. With known Φ_p, the Fourier coefficients are calculated as $\mathbf{F} = |\varphi_d|\mathbf{M}\Phi$. The potential distribution at the second ($y = T_1$) interface, which may be of separate interest, can be found from eq 14.

1.2. Prediction of the Sensor Admittance, $\mathbf{Y}_{sen}$. For spatially periodic IDE sensors, if we ignore the thickness of sensor electrodes, eq 4 is simplified to the following expression (cf. eq 4 of ref 16):

$$\mathbf{Y}_{sen} = \frac{j\omega\epsilon_0 N_e L_{sen}}{|\varphi_d|}\int_{3L/4}^{L}[\epsilon^*_{sub}\,E^b_{y(1)} - \epsilon^*_{fut}\,E^a_{y(1)}]\,dx \quad (23)$$

where N_e is the total number of IDE electrodes and L_{sen} is the electrode length in z direction. Using the derived expressions for $E^a_{y(1)}$ and $E^b_{y(1)}$, after the integration, we obtain

$$\mathbf{Y}_{sen} = \frac{j\omega\epsilon_0 N_e L_{sen}}{|\varphi_d|}[\epsilon^*_{sub}\mathbf{D} + \epsilon^*_{fut}\mathbf{C}]\mathbf{F}$$

$$= j\omega\epsilon_0 N_e L_{sen}[\epsilon^*_{sub}\mathbf{DM} + \epsilon^*_{fut}\mathbf{CM}]\Phi \quad (24)$$

where the elements of the complex matrix $\mathbf{C} \in \mathcal{C}^{1\times(m+1)}$ and the real matrix $\mathbf{D} \in \mathcal{R}^{1\times(m+1)}$ are equal to

$$C_{1,n+1} = s_n \sin\left(k_n\frac{3L}{4}\right) \quad (25)$$

$$D_{1,n+1} = \coth(k_n T_{sub})\,\sin\left(k_n\frac{3L}{4}\right) \quad (26)$$

(16) Choi, Y.-H.; Skliar, M. *Anal. Chem.* **2004**, *76*, 4143.

With known ϵ^*_{fut}, ϵ^*_{sil}, and ϵ^*_{sub}, eq 24 gives the prediction of the IDE sensor admittance as a function of the FUT thickness, T_1.

1.3. Stray Contributions. The impedance contribution of stray elements can be estimated by comparing the theoretical prediction of the sensor impedance, $1/\mathbf{Y}_{sen}(T_1)$, calculated using eq 24 for the FUT of known thickness and ϵ^*_{fut}, with the corresponding measured sensor impedance:

$$\mathbf{Z}_{stray} = \left[\frac{1}{\mathbf{Y}_m} - \frac{1}{\mathbf{Y}_{sen}(T_1)}\right] \quad (27)$$

The estimated $\mathbf{Z}_{stray}$ is later used to adjust for stray contributions the predictions and the measurements of the sensor admittance with the FUT of an unknown thickness.

2. Estimation of the Film Thickness. Assume that dielectric permittivities ϵ^*_{fut}, ϵ^*_{sil}, and ϵ^*_{sub} are isotropic and known. The following steps summarize the proposed method for noninvasive measurement of dielectric film thickness using FE sensors of a given periodic design:

1. Estimate stray contributions as described in the Stray Contributions section. Equation 27 allows us to estimate $\mathbf{Z}_{stray}$ based on $\mathbf{Y}_m(\omega)$ measurements and the corresponding $\mathbf{Y}_{sen}(T_1;\omega)$ predictions for the FUT of any known thickness. It may be convenient to estimate strays when $T_1 = 0$, before the film is formed.

2. Use eq 24 to predict sensor admittance, $\mathbf{Y}_{sen}$, at frequencies ω_i as a function of T_1. This prediction is the most computationally intensive part of the method. Then, use eq 2 to adjust $\mathbf{Y}_{sen}$ for the stray contribution, $\mathbf{Z}_{stray}$, to obtain $\mathbf{Y}'_{sen}$. Note that steps 1 and 2 may be carried out off line, before the measurements of an unknown film thickness are started.

3. Probe the FUT of unknown thickness by measuring $\mathbf{Y}_m$ of the FE sensor at selected excitation frequencies, ω_i, $i = 1,..., N_f$.

4. Compare the stray-adjusted prediction, $\mathbf{Y}'_{sen}(\omega_i)$, with the measured $\mathbf{Y}_m(\omega_i)$. At each frequency, determine T_1, which minimizes the difference between $\mathbf{Y}'_{sen}$ and $\mathbf{Y}_m$. The least-squares estimate of the film thickness, $\bar{T}_1$, is the average of the results at different excitation frequencies:

$$\bar{T}_1 = \frac{1}{N_f}\sum_{i=1}^{N_f} T_1(\omega_i) \quad (28)$$

5. The measurements of the time-varying film thickness (due to growth, degradation, cyclic change, or any other reason) are obtained by repeated execution of steps 3 and 4.

The theoretical prediction of the sensor admittance (direct problem, step 2) in the general case of FE sensors of arbitrary design, configuration, and electrode geometry (including the case of nonplanar, curvilinear, and flexible substrates) must be based on the general eq 4 and will require numerical calculation of nonuniform, three-dimensional excitation field, $\mathbf{E} = (E_x, E_y, E_z)$.

The experimental validation with low-loss dielectric film, described below, uses a particular embodiment of the developed method, which estimates the film thickness (step 4) by minimizing

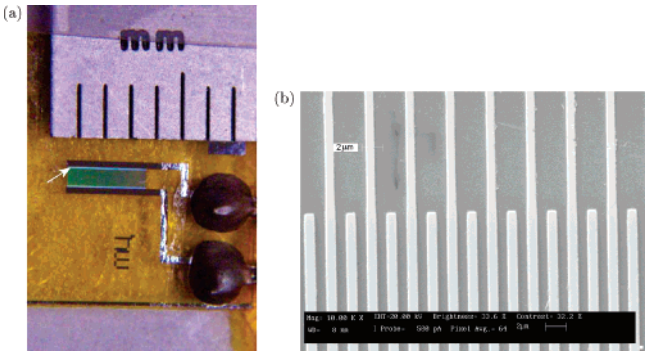

Figure 2. (a) IDE sensor used in experiments; (b) SEM micrograph of the area indicated by the arrow in (a).

the error between the measured capacitance, $C_m(\omega_i)$ and its stray-adjusted prediction given by

$$C'_{sen}(T_1) = \frac{1}{\omega}\mathrm{Im}[\mathbf{Y}'_{sen}(T_1)] \tag{29}$$

Equations 24, 2, and 29 are used off-line to create a lookup table for C'_{sen} as a function of frequencies and T_1. The time-varying film thickness is then estimated by interpolating between table entries to match the measured capacitance, $C_m(\omega_i)$.

EXPERIMENTAL VALIDATION

The developed method was tested using an IDE sensor (MS-01, Netzsch Instruments, Burlington, MA, Figure 2), consisting of 1500 ($N_e = 2 \times 750$) chromium electrodes microfabricated on a quartz substrate. The electrode spacing, length (L_{sen}), width, and L are 1, 800, 1, and 2 μm, respectively. At the beginning of the experiments, the sensor was cleaned in piranha solution, rinsed with deionized water, and dried. The admittance, capacitance, and resistance spectra were measured using a precision LCR meter (HP 4284A, Agilent Technologies, Palo Alto, CA) in the range of excitation frequencies from 10^3 to 10^5 Hz.

The dielectric permittivity of the sensor substrate was obtained experimentally. One MS-01 sensor was sacrificed to form a parallel plate (PP) capacitor by vacuum sputter deposition of chromium on both sides of the sensor substrate. The permittivity ϵ^*_{sub} was calculated from the measurements of the dissipation factor and capacitance of the formed PP capacitor, which were acquired using the parallel plate test fixture (HP 16451B, Agilent Technologies).

A silicon nitride film of unknown thickness T_1 was deposited on the surface of the IDE sensor in 12 increments by rf magnetron sputtering (Discovery 18 DC/RF Research Magnetron Sputter Deposition System, Denton Vacuum, Moorestown, NJ) of 99.9% pure silicon nitride target (Kurt J. Lesker Co., Clairton, PA). A microscope slide, partially covered by an acrylic adhesive tape, was placed inside the sputtering chamber in the immediate proximity of the sensor. By the experimental design, the thickness of the silicon nitride layer on the microscope slide and the IDE sensor were the same.

After each incremental deposition of silicon nitride, we measured the following:

1. New thickness of the silicon nitride layer on the microscope slide. The thickness was measured using contact profilometer (Dektak III surface profiler, Veeco, Woodbury, NY) as the average difference in surface levels of areas covered by the tape and exposed to sputtering.

2. The capacitance $C_m(\omega_i)$ and resistance $R_m(\omega_i)$ of the IDE sensor. The corresponding sensor admittance is given by eq 3. The measured C_m as a function of the number of deposited layers and the excitation frequency $f = \omega/2\pi$ is plotted in Figure 4.

RESULTS

The measured permittivity of the sensor substrate, ϵ^*_{sub}, is shown in Figure 3a as the dielectric storage, ϵ'_{sub}, and loss, ϵ''_{sub}, spectra.

The stray contribution, $\mathbf{Z}_{stray}$, was estimated from eq 27 by comparing the measured admittance, $\mathbf{Y}_m$, of the sensor before FUT was deposited ($T_1 = 0$) with the corresponding to theoretical prediction, $\mathbf{Y}_{sen}(T_1 = 0)$, given by eq 24. The prediction was calculated using the measured substrate permittivity, ϵ^*_{sub}, and assuming that $\epsilon^*_{sil} = 1$, which is a good approximation for the dry air. The result in the form of the real and imaginary parts of $\mathbf{Z}_{stray}$ is shown in Figure 3b.

The dielectric permittivity of the FUT material, ϵ^*_{fut}, must be known to predict the sensor admittance. We did not assume that ϵ^*_{fut} is equal to the permittivity of the sputtering target, because the properties of the dielectric films, deposited by sputtering, are known to depend on processing conditions. Instead, we continued the incremental deposition of silicon nitride until $\mathbf{Y}_m$ (and C_m) saturated with the number of depositions and became insensitive to further increase in T_1. The measurements of C_m as a function of incremental depositions, seen in Figure 4, agrees with the theoretical expectation that the sensor admittance for $T_1/L \gg 1$ is essentially equal to the sensor admittance when $T_1 \to \infty$. We, therefore, assumed that after the final 12th incremental deposition, which increased the FUT thickness to $\sim 3L/2$, the contribution of the semi-infinite layer of dry air to the measured $\mathbf{Y}_m$ can be ignored, and we effectively have a case of the semi-infinite silicon nitride layer on the sensor substrate. The dielectric permittivity of FUT, ϵ^*_{fut}, was then obtained using the method described in ref 15. The results are shown in Figure 3c.

With known permittivities (ϵ^*_{sub}, ϵ^*_{fut}, ϵ^*_{sil}), the sensor admittance, $\mathbf{Y}_{sen}$, was predicted as a function of the FUT thickness, as described in the Prediction of the Sensor Admittance Section. The predictions were obtained by retaining the first 50 components in the series solution for the electric field ($m = 50$), and the result was adjusted for the stray contribution. The stray-adjusted prediction of the sensor capacitance was obtained according to eq 29.

After each incremental deposition, the new value of $T_1(\omega_i)$ was found by matching the stray-adjusted predictions of the sensor capacitance, $C'_{sen}(T_1)$, to the direct capacitance measurements, C_m. The process, illustrated by Figure 4, was repeated for all ω_i.

The frequency-averaged result, $\bar{T}_1$, is plotted in Figure 5, where the error bars indicate the standard deviation of T_1, estimated at different frequencies. The comparison with the direct, profilometer measurements shows an excellent agreement of the developed methods with the independent thickness measurements when the film thickness is less than $\sim(2/3)\ L$. The admittance measurements become insensitive to changing film thickness when T_1 becomes large relative to the electrode spacing, L.

DISCUSSION

The developed method estimates the unknown thickness of a dielectric film by minimizing the difference between the measured

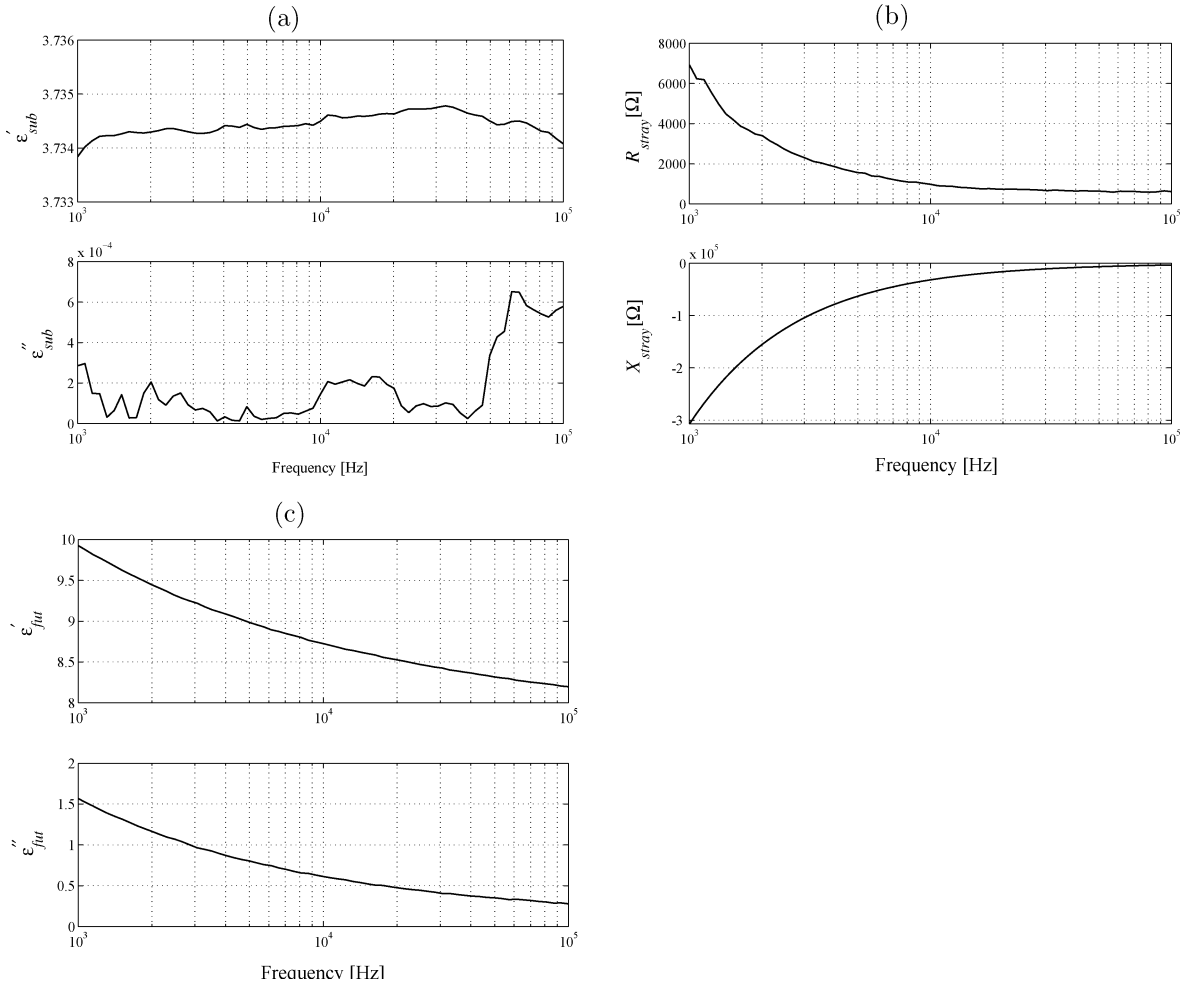

Figure 3. (a) Dielectric permittivity of the sensor substrate: $\epsilon^*_{sub} = \epsilon'_{sub} - j\epsilon''_{sub}$; (b) series stray impedance, $\mathbf{Z}_{stray} = R_{stray} + jX_{stray}$; (c) dielectric permittivity of the silicon nitride film, $\epsilon^*_{fut} = \epsilon'_{fut} - j\epsilon''_{fut}$.

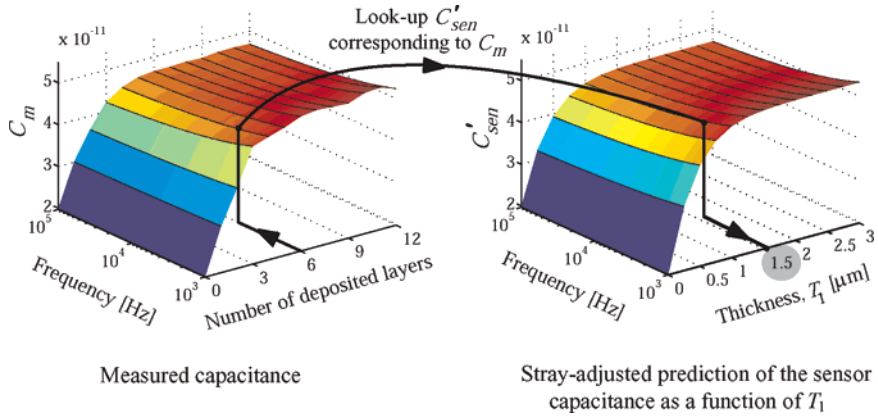

Figure 4. $C''_{sen}(T_1)$ entry of the tabulated values of the stray-adjusted prediction of the sensor capacitance selected equal to the measured capacitance, C_m. The corresponding T_1 gives the estimate of an unknown film thickness.

and predicted passive electrical properties of the FE sensor located at the film interface. In one implementation, after accounting for the contribution of stray elements, the film thickness is obtained by matching thickness-dependent predictions and measurements of FE sensor admittance. In the general case of an arbitrary configuration of interfacial electrodes, used to create the fringing electrical field inside the FUT, the numerical solution of the direct and inverse problems may be computationally expensive to obtain. However, for FE sensors of periodic, interdigitated electrode configuration, the implementation is significantly simplified and is suitable for the real-time measurements of rapidly evolving film thickness.

The maximum measurable film thickness is determined by the spacing of the sensor electrodes. In the case of IDE sensors, the maximum measurable T_1 is controlled by the characteristic distance, L, between centers of adjacent electrodes. Consequently, the upper range of thickness measurements can be easily tailored to the specific needs by selecting a sensor with an appropriate L.

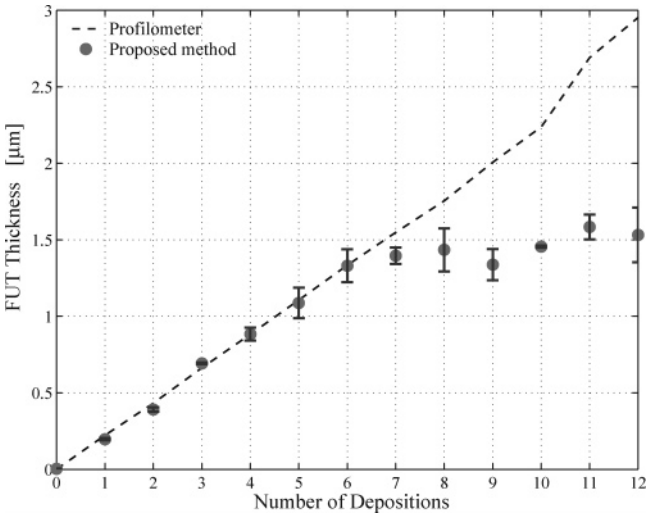

Figure 5. Measured film thickness.

The strong influence of the electrode spacing on the range of sensor sensitivity is explained by eq 7, which indicates that the strength of the probing electric field in the direction normal to sensor−film interface decays exponentially (approximately as $\exp(-T_1/L)$). The experimental results of Figure 5 show that it was possible to accurately measure the FUT thickness for $T_1 \leq (2/3)\ L$.

The minimum measurable film thickness is limited by the measurement noises and the accuracy of the admittance measurements. If instrumental accuracy and the measurement noise are not the constraining factors, then the effect of the nonzero height of the sensor electrodes (typically in the nanometer range for microfabricated FE sensors) must be taken into the account. This can be done by accounting for the contribution of the parallel plate capacitor, formed by the FUT material between the electrodes of a finite height, to the prediction of the sensor admittance.

The dynamic range (defined as the ratio of maximum to minimum measurable film thickness) may be improved by using an array of FE sensors with different L. The improved dynamic range may also be achieved using a single sensor with addressable electrodes, thus allowing us to select electrode spacing equal to $I_{nt}L$, where I_{nt} is an integer. Note, however, that, by increasing I_{nt}, the overall sensor admittance will decrease because of the following factors: (1) The admittance of any two further separated driven-sensing electrodes is smaller; (2) The number of active FE electrode pairs, contributing to the overall sensor admittance, will decrease. Therefore, an increased I_{nt} will lead to a decreased signal-to-noise ratio.

Compared to the alternative techniques, the following features make the developed method attractive for measurements of film thickness in confined and inaccessible locations (such as inside an equipment or a tool, test cell, or in vivo), and substrates of complex geometry:

1. The FE sensors are embedded into the film substrate and provide in situ thickness measurements.

2. The method can be used with an arbitrary and time-varying orientation of the substrate−film interface (as in the case of a film on moving surfaces). Thickness measurements at the interface of changing spatial location is a difficult problem to overcome with alternative methods.

3. The developed method is applicable when the substrate is not planar. For example, an FE sensor, fabricated on the inner surface of a conduit, can be used to measure an evolving film thickness on the inside of an open or enclosed channels of an arbitrary geometry.

4. By fabricating the FE sensor on a flexible substrate, the developed method can be used to measure film thickness on surfaces of changing geometry.

5. With multiple embedded FE sensors, the film thickness in different spatial locations can be simultaneously measured.

Another advantage of the developed method is the ability to simultaneously measure the film thickness and the dielectric permittivity of the FUT. This is especially important when a film material undergoes transformation due to aging, diffusion, chemical reaction, or any other reason that alters its dielectric properties. As an illustration of this capability, consider an array of FE sensors and assume that one of the sensors in the array has electrode spacing, L, that is small relative to the measurement range of T_1. To a good approximation, the admittance of this sensor will be the same as if the FUT had an infinite thickness, and the method of ref 15 can be used to measure ϵ^*_{fut} as a function of time. With this information, the remaining sensors in the array can be used to measure the time-varying film thickness.

The experimental testing of the developed method has revealed that the incrementally increasing thickness of the silicon nitride film is accurately measured in the expected range of the IDE sensor sensitivity, $T_1 \leq (2/3)\ L = 4/3\ \mu$m. The ability to simultaneously measure T_1 and ϵ^*_{fut} was demonstrated by first, measuring the film permittivity when thickness exceeded the measurable range of the sensor and then using this information to reconstruct the history of evolving film thickness based on the admittance measurements, taken after each consecutive deposition, starting with $T_1 = 0$.

The experimental demonstration of the developed method was for the case of a low-loss dielectric film. Because of high FUT resistance, the measurement of thickness was based on matching thickness-dependent prediction of sensor capacitance with the measured value. When FUT material is lossy, the thickness measurement may be based on matching the predication of the FE sensor resistance with the corresponding resistance measurements. For certain materials, it may be advantageous to estimate T_1 based on both imaginary and real parts of the sensor's admittance.

The developed method is only applicable when the FUT and the media in which it develops have dissimilar dielectric storage, loss spectra, or both.

ACKNOWLEDGMENT

This research was supported by the National Science Foundation (Grant CTS-9875462).

Note Added after ASAP Publication. This paper was posted on April 7, 2006 before a correction to eq 4 (S subscript to the integral sign) was made. The correction was completed, and the paper was reposted on April 17, 2006.

Received for review May 4, 2005. Accepted February 14, 2006.

AC050770Z